Measurement and simulation of viscous dissipation rates in the wave affected surface layer

Adolf Stips, [a,*]

Hans Burchard, [b]

Karsten Bolding, [c]

Hartmut Prandke, [d]

Alfred Wüest [e]

[a] *CEC Joint Research Centre, Institute for Environment and Sustainability, I-21020 Ispra(VA), Italy*

[b] *Institute for Baltic Sea Research, Universität Rostock, Seestrasse 15, D-18119 Rostock, Germany*

[c] *Bolding & Burchard Hydrodynamics GbR, Strandgyden 25, DK 5466 Asperup, Denmark*

[d] *ISW Wassermesstechnik Dr. Hartmut Prandke, Lenzer Str. 5, D-17213 Petersdorf, Germany*

[e] *Applied Aquatic Ecology, EAWAG, CH-6047 Kastanienbaum, Switzerland*

Abstract

In this study we compare turbulence parameters from field observations and model simulations specifically under the influence of weak to moderate wind forcing and

breaking short waves. The experiment was performed during 12 days under very weak stratification at a fetch limited lake in Switzerland. The near surface observations were obtained by using a quasi-free rising profiler which measured small scale shear and temperature fluctuations. We used a state-of-the-art two-equation k-ϵ turbulence model with an algebraic second-moment closure scheme. The one-dimensional numerical model was extended to consider breaking waves by a shear-dependent closure for the second moments.

The agreement of the turbulence quantities resulting from observations and simulations is very promising. Especially well simulated is the enhanced turbulence level in the wave-affected-surface-layer (WASL) of a few dm thickness. The logarithmic slope of the turbulent dissipation rate in this WASL was found to vary between -2.1 and -1.7. Below the WASL the classic *law-of-the-wall* was well reproduced by the data and the model.

Key words: Turbulence Measurements, Numerical Modelling, Wave Breaking, Dissipation Rates

---

* Corresponding Author
Email address: adolf.stips@jrc.it (Adolf Stips,).

1 Introduction

The surface boundary layer (SBL) of natural waters is a corner stone of earth sciences. Understanding and adequate parameterisation of heat, gas and momentum exchange with the atmosphere - especially under breaking waves - is fundamental for the physical and biogeochemical processes in oceans, lakes and reservoirs.

The early measurements in lakes (Thorpe (1977), Dillon et al. (1981)) and oceans (Lombardo and Gregg (1989)) revealed regularly logarithmic velocity profiles with rates of dissipation ε of turbulent kinetic energy (TKE) increasing proportional to the inverse of depth. Subsequently, the first adopted SBL turbulence model was the concept of the *law-of-the-wall* (LOW), which is a special case of the Monin-Obukhov theory (Monin and Obukhov (1954), Businger et al. (1971)) for zero vertical buoyancy flux.

As experimental techniques improved and turbulence could be measured with better spatial and temporal resolution a more realistic and consistent picture of the top 1 m of the SBL emerged. In the uppermost layer, Kitaigorodskii et al. (1983) found turbulence levels to depend on the surface wave energy with dissipation rates being one or two orders of magnitude above those predicted by LOW. It was shown extensively in Lake Ontario that this extra turbulence is injected by breaking waves (Agrawal et al. (1992), Terray et al. (1996), Drennan et al. (1996), Donelan (1998)). Measurements in the ocean by upward-operated microstructure profilers (Anis and Moum (1992), Anis and Moum (1995), Lass and Prandke (2003)), profiling surface buoys by Gemmrich and Farmer (1999) and Gemmrich and Farmer (2004) and by horizontally

manoeuvred submarines (Osborn et al. (1992), Thorpe et al. (2003)) strengthened the view that within several significant wave heights (typically < 2 m) the dissipation rate is at least an order of magnitude above LOW levels. Dissipation was found specifically concentrated in bubble clouds. This so-called wave-affected-surface-layer (WASL) was found to consist of a two-layer structure (Terray et al. (1996)). According to their model, approximately half of the TKE dissipation occurs in the very top, so-called wave-turbulent sublayer (Benilov and Ly (2002)), where TKE injection by wave breaking dominates, production by shear is comparably negligible and ε is approximately constant. Below this depth, there is a transition-turbulent sublayer, where the vertical diffusion of TKE still exceeds the local shear production. There dissipation rates scale with wind-wave parameters and ε has logarithmic slopes of -2.3 ± 0.4, depending on the wave height and the wave age. Below, the transition-turbulent sublayer merges with the LOW layer, where turbulence production and dissipation are in balance.

SBL modelling is thus challenged by this complexity of the SBL (Zhang and Chan (2003)). Craig and Banner (1994) and Craig (1996) employed an improved level-2.5 closure model to reproduce the observed SBL turbulence. The effect of wave breaking has been modelled by a TKE flux into the surface. By prescribing the macro (integral) length scale from LOW scaling, they could even show an analytical solution which combines the WASL on top of the LOW including the transition zone in between those two layers. Recently, Burchard (2001a) incorporated those ideas in an extended k-ε turbulence model, allowing to simulate the dynamics in the WASL on top of the logarithmic layer, which is properly reproduced by unmodified k-ε models.

Since it is arbitrary and empirically not proven that the macro length scales

the same way in the WASL and under LOW conditions, Umlauf and Burchard (2003) developed a generic two-equation model which allows for different length scale slopes in both regimes. This was motivated by observations in grid-generated, shear-free turbulence, where the length scale had slopes of $L = 0.2$ rather than the van Karman parameter of $\kappa = 0.4$ as under LOW conditions. Recently, Kantha and Clayson (2004) extended the k-kl model by Mellor and Yamada (1982) such that the effects of surface wave breaking on near-surface turbulence is reproduced by that model as well. Their model predicts a length scale slope ratio of $\kappa/L = 1.8$, a value which is close to some laboratory data from grid stirring experiments. However, due to the uncertainty whether grid stirring experiments are a good model for surface wave breaking, we use here the model by Burchard (2001a) with $\kappa = L = 0.4$.

Apart from the near-surface length scale slope, two other model parameterisations for surface wave breaking are of scientific debate: the height of the unresolved wave-turbulent sublayer, z_0 and the surface flux of TKE, $F_s(k)$. For the latter, usually $F_s(k) \propto |u_*|^3$ (with the surface friction velocity u_*) is used, where the parameter of proportionality may depend on wave age (see Terray et al. (1996), Terray et al. (1999)). However, often a constant parameter of proportionality is chosen, as in e.g. Craig and Banner (1994). Depending on the observational technique for near-surface turbulence, various parameterisations have been suggested for z_0. Based on observations from fixed towers where the surface reference is the mean surface elevation, Terray et al. (1999) suggest $z_0 = H_s$ with the significant wave height H_s. In contrast to that, Gemmrich and Farmer (1999) find much smaller values for z_0 with an instrument floating with the waves and thus having the momentary sea surface as the reference. For significant wave heights of about 5 m, they found $z_0 \approx 0.2$

m, see also Gemmrich and Farmer (2004) who confirmed that result. Using a freely-rising profiler equipped with a pressure sensor, as in the present study, will also allow reference to the momentary surface elevation, and thus z_0 to H_s ratios similar to Gemmrich and Farmer (1999) are expected.

In this paper we aim at two goals: Firstly we present microstructure data of the SBL from a fetch-limited wind-exposed lake, where significant turbulence has been observed (Simon (1997); Sander et al. (2000); Lorke and Wüest (2002)). It will be shown that also for this special situation of short and young breaking waves there exists a well-defined WASL with enhanced dissipation. In addition, we thereby demonstrate that the often criticised profiling method (Gibson (1982)) captures the WASL despite the large intermittency. Until now, practically only Anis and Moum (1995) used the vertical profiling technique for this purpose. Secondly, we want to test whether the improved model by Burchard (2001a) is also able at reproducing the turbulence measurements taken under those specific conditions of short and young waves. As an additional test, we investigate specifically the lower range of wind speeds and examine the slope of turbulent dissipation rate in the WASL. As the unmodified $k-\varepsilon$ model has been many times tested rigorously against different sets of measurements (Burchard and Bolding (2002), Stips et al. (2002), Simpson et al. (2002)), we clearly refrain from any tuning of parameters of the model itself.

The improved two-equation k-ε turbulence model by Burchard (2001a) is explained in section 2, the measurement setup is described in section 3, whereas the data from the measurements and from the simulations are presented in section 4, before they are finally discussed in section 5.

2 Model description

The mathematical model on which the numerical simulations are based here, consists of six dynamical equations for the two Reynolds averaged velocity components u (eastward) and v (northward), the averaged potential temperature T, the averaged salinity S, the turbulent kinetic energy k and the turbulent dissipation rate ε:

$$\begin{aligned}
\partial_t u - \partial_z((\nu_t + \nu)\partial_z u) &= fv, \\
\partial_t v - \partial_z((\nu_t + \nu)\partial_z v) &= -fu, \\
\partial_t T - \partial_z((\nu_t' + \nu')\partial_z T) &= \frac{1}{C_p \rho_0}\partial_z I, \\
\partial_t S - \partial_z((\nu_t' + \nu'')\partial_z S) &= 0, \\
\partial_t k - \partial_z\left(\frac{\nu_t}{\sigma_k}\partial_z k\right) &= P + B - \varepsilon, \\
\partial_t \varepsilon - \partial_z\left(\frac{\nu_t}{\sigma_\varepsilon}\partial_z \varepsilon\right) &= \frac{\varepsilon}{k}\left(c_1 P + c_3 B - c_2 \varepsilon\right),
\end{aligned} \tag{1}$$

with gravitational acceleration g, averaged density ρ and the Coriolis frequency

$f = 2\omega \sin(\phi)$ with the earth's angular velocity ω and latitude ϕ. In the potential temperature equation, further terms are solar radiation I in the water column (generally calculated from the given surface radiation as an exponentially decreasing function with depth), the specific heat capacity of sea water C_p, and a reference density ρ_0. The molecular diffusivities for momentum, temperature and salinity are given by ν, ν' and ν'', respectively. The coordinates are x (eastward), y (northward), z (upward) and t (time). In addition to the system of equations (1), the UNESCO equation of state for calculating the potential density as functions of T, S and hydrostatic pressure is applied. Shear production of turbulence is denoted as $P = \nu_t \left((\partial_z u)^2 + (\partial_z v)^2\right)$ and buoyancy production as $B = \nu_t'(g\rho_0)\partial_z \rho$. Eddy viscosity and eddy diffusivity are denoted by ν_t and ν_t', respectively.

The first four equations of (1) for velocity components and active tracers are the so-called hydrostatic primitive equations with some further simplifications. Horizontal homogeneity is assumed with the consequence that all horizontal gradients such as pressure gradients and advective terms vanish. It will be discussed later that this assumption is crude near the shore, but however necessary due to lacking information on such gradients.

The turbulence closure needed to calculate ν_t and ν_t' is obtained from applying a Reynolds decomposition into a mean and a fluctuating part of the flow and tracer fields and to construct transport equations for the second-order correlators of fluctuations. After assuming local equilibrium for these correlators and closing remaining unknowns by empirical assumptions, eddy viscosity and diffusivity result as (Burchard (2002)).

$$\nu_t = c_\mu \frac{k^2}{\varepsilon}, \qquad \nu_t' = c_\mu' \frac{k^2}{\varepsilon}. \tag{2}$$

Here, c_μ and c_μ' are non-dimensional stability functions, depending on shear frequency, Brunt-Väisälä frequency and the turbulent time scale, k/ε. We use here the set of stability functions which has recently been suggested by Canuto et al. (2001) and validated against mixed layer observations by Burchard et al. (2000).

The equations for turbulent kinetic energy k and its dissipation rate ε are needed for two reasons: (i) calculating the vertical eddy viscosity and diffusivity ν_t and ν_t' by means of (2) and (ii) reproducing the observed dissipation rate ε. These equations for k and ε result from the Reynolds decomposition discussed above.

Starting from the standard prognostic equation for turbulent kinetic energy (fifth equation of (1)), Craig and Banner (1994) suggested an analytical solution for the wave enhanced layer by assuming a positive surface flux of TKE due to energy injection by breaking surface waves and a balance of viscous dissipation with vertical TKE transport (thus neglecting shear production of TKE). Since this is realistic only very close to the surface, Craig (1996) extended this study by including shear production for which he found an approximate analytical solution. When prescribing the macro length scale as $l = \kappa d$ with the non-dimensional distance $d = (z_0 - z)/z_0$ from below an unresolved surface layer of thickness z_0 (with the vertical coordinate z pointing upwards) and prescribing the surface TKE flux as $F_s(k) = c_w |u_*|^3$ (with the empirical non-dimensional parameter c_w and the surface friction velocity u_*)

the analytical solution including the WASL reads as

$$k_{WASL} = k_{LOW}\left(1 + c \cdot d^{-m}\right)^{2/3}$$

$$\varepsilon_{WASL} = \varepsilon_{LOW}\left(1 + c \cdot d^{-m}\right) \tag{3}$$

with the empirical non-dimensional parameters m and $c \propto c_w$. Here, $k_{LOW} \propto u_*^2$ and $\varepsilon_{LOW} \propto |u_*|^3 d^{-1}$ denote the LOW solutions. Since the spatial decay of ε_{LOW} is $\propto d^{-1}$, the decay of ε_{WASL} near the surface is given as $\propto d^{-(m+1)}$. The parameter m depends on the Schmidt number for TKE, σ_k, the van Karman parameter κ and the ratio of surface friction velocity squared to TKE, c_μ. Using standard parameters for the TKE equation from various sources (e.g. Mellor and Yamada (1974), Rodi (1980)), the spatial decay rate $-(m+1)$ falls into the empirical range of -2.3 ± 0.4. For the Canuto et al. (2001) stability functions however, $-(m+1) = -3.2$ (see section 7) which is outside the empirical range, but only very close to the surface, where shear is negligible.

The parameters contained in the ε equation are fitted to various empirical laws, see Umlauf and Burchard (2003) for a review. One of them, the Schmidt number σ_ε is fitted such that the LOW is a solution for steady-state constant stress conditions. It could however also be fitted to pure WASL conditions (no shear production), but then the LOW conditions would be excluded. Since the parameters c_1 - c_3 are already used for reproducing other flow properties, no more degree of freedom is left for including the WASL and LOW conditions in one model. Since pure WASL conditions are characterised by $P/\varepsilon \to 0$ and pure LOW conditions by $P/\varepsilon = 1$, Burchard (2001a) suggested to calculate

the Schmidt number for ε as

$$\sigma_\varepsilon = \max\left\{0, 1 - \frac{P}{\varepsilon}\right\}\sigma_{\varepsilon,WASL} + \min\left\{1, \frac{P}{\varepsilon}\right\}\sigma_{\varepsilon,LOW} \tag{4}$$

and could show that the resulting numerical solution approximated the Craig (1996) analytical solution very well.

The present turbulence model uses the empirical parameters given in table 1. The turbulent Schmidt number for the turbulent kinetic energy, $\sigma_k = 1$ is a rough estimate (see e.g. Rodi (1980)), the turbulent Schmidt numbers for the dissipation rate, $\sigma_{\varepsilon,WASL}$ and $\sigma_{\varepsilon,LOW}$ depend on various other parameters (see section 7), c_1 and c_2 result from laboratory experiments with homogeneous shear flow and grid turbulence, respectively. For stable stratification, c_3 results from fitting the steady-state Richardson number to idealised experiments (see Burchard and Baumert (1995), Burchard et al. (2000)), for instable stratification, c_3 needs to be positive in order to retain a source of dissipation rate also for free convection, see Rodi (1980). In order to obtain positive definite solutions for the stability functions c_μ and c'_μ, certain realisability constraints have to be considered, see Burchard and Deleersnijder (2001).

The numerical discretisation of the model is described in detail by Burchard et al. (1999) and Umlauf et al. (2004). In order to obtain numerically stable results for this strongly convective scenario, a time step of $\Delta t = 10$ s has been used. The vertical resolution was not equidistant, as we used slight zooming to the surface. The mean vertical step size was about $\Delta z = 0.15$ m. The model was initialised on March 9 1996 at 00:00 h with the first observed profiles of temperature and salinity (section 3), zero velocities and k and ε set to minimum values. The model simulation terminates on March 20 at 13:00 h

when the last vertical profile was observed.

For doing the simulations the height of the unresolved wave-turbulent sublayer z_0 (also called surface roughness length) has to be prescribed as additional external model parameter. As Burchard (2001a) has shown that an adaptation of the Charnok (1955) formula

$$z_0 = \alpha \, u_*^2 / g \tag{5}$$

with the dimensionless parameter $\alpha = 1400$, Craig and Banner (1994), resulted in a satisfactory simulation of available observations, we also used equation 5 as a starting point for the simulations. Further we investigated the sensitivity of the model to the roughness length z_0, by using different values for the parameter α (e.g. 5600, 14000, 56000).

3 Observations

3.1 Study site and experimental setup

The measurements were carried out in Lake Neuchâtel, located in the western part of the Swiss Plateau. The lake is quasi-rectangular, with its longest axis directed SW-NE. It has a volume of 13.8 km^3, a surface of 214 km^2 and a maximum depth of 153 m. The largest inflow is coming from the river Areuse, located 30 km NE of our measurement site. The experiment took place during 12 days from March 9 to 20, 1996. We have chosen a measurement place located at the shore of Chez le Bart (46^o 53,883' N, 6^o 47,383' E, figure 1). The particular location for the experiment was selected for its wind exposure, the absence of major river inlets and a steep shore line to allow the safe mooring of the instrumentation (Simon (1997)).

In order to measure the atmospheric forcing, wave heights and turbulence, we operated a meteorological station on a buoy $\approx$2 km off-shore and a moored pressure gauge and two microstructure profilers $\approx$300 m off-shore, see figure 1. The profilers were placed at a water depth of 38 m. The sampled depth interval ranged from 30 m up to the surface. Meteo data (wind speed, wind direction, buoy orientation, air temperature, relative humidity, solar radiation and global radiation) were measured by an autonomous meteo station AMS 2700 (Aanderaa Instruments, Bergen, Norway) at 2.8 m height above lake surface every 2 minutes. Near to the location of the microstructure probes an additional anemometer was placed at 0.95 m above lake surface (figure 1).

Microstructure profiles were collected by using two completely different probes,

sensing small-scale temperature and current shear (see below). This allowed to infer and compare dissipation of TKE from two independent systems (Kocsis et al. (1999)). These probes were connected via special winches to data acquisition and control computers at the shore base. For general background information thermistor strings and current meters were moored. The positions of the respective instruments, as well as their denomination in figure 1 is detailed in table 2.

3.2 Microstructure measurement technique

Two profilers were operated in quasi freely-rising mode, to infer TKE dissipation rates: The MST profiler of the Joint Research Centre (Ispra, Italy) (predecessor of the MSS profiler as produced by Sea & Sun Technology and ISW Wassermesstechnik, Germany) and a temperature microstructure profiler based on SeaBird (Bellevue, USA) sensors and electronic boards, owned by EAWAG.

The MST profiler was equipped with microstructure temperature and current shear sensors, as well as conventional CTD-sensors. The microstructure temperature sensor is based on a microthermistor FP07 (Thermometrics, USA) with a nominal response time of about 7 ms. For the microstructure shear measurements, the profiler was equipped with a PNS shear sensor (Prandke and Stips (1998)). The standard temperature sensor is of the Pt100 type and has an accuracy of ± 0.01 ^{o}C. For the electrical conductivity measurements a 7-pole cell with an accuracy of ± 0.01 mS/cm is used. The piezo-resistive pressure sensor has an accuracy of ± 10 cm. The resolution for all sensors is determined by the used 16 Bit analog digital converter. The sampling rate

for all sensors was 1024 per second. The system enables the measurement of small-scale current shear with a vertical resolution down to about 5 mm. The mechanical construction, the electronics and the basic signal processing are described in detail by Prandke and Stips (1998) and in the references cited therein.

The temperature microstructure profiler is an adapted SeaBird SBE-9 CTD profiler. It was equipped with a pair of FP07 thermistors. The sampling frequency was 96 Hz. Details of the profiler construction as well as the processing and analysis of the temperature microstructure data are described in Simon (1997), Kocsis et al. (1999) and Lorke and Wüest (2002).

For the rising measurements the winch was placed at the shore and a guide pulley was used about 300 m away from the shore at a water depth of 38 m. To reduce the influence of cable vibrations on the profiler, the cable of the MST profiler was pulled by an additional buoyancy ball equipped with a pressure sensor, at about 6 m below the profiler. Data were recorded between 30 m and 0 m depth. One single cast was done every 15 minutes, resulting in a total of more than 1100 casts.

Dissipation rates from both profilers were found to agree satisfactory (Kocsis et al. (1999)). There from it can be concluded that the temperature microstructure method using standard thermistors, is very suitable for resolving very low dissipation rates (smaller 10^{-10} m^2s^{-3}), but seems to underestimate dissipation rates above 10^{-7} m^2s^{-3}. As the focus of this work is the very near surface region having higher dissipation rates, we decided to use here the dissipation rate data from the MST profiler alone.

3.3 MST data processing and reduction

The shear data processing followed the commonly used procedure for shear calculation as described by Stips and Prandke (2000). Spiky data were detected and removed by a filter which determines the local variance of the signal. Thereafter a bandpass filter was applied to remove low frequency disturbances as well as high frequency noise. Overlapping depth segments of 0.3 m length were used to calculate the shear variance and to estimate the dissipation rate ε. For the spectrum integration the lower wavenumber bound k_L is 2 cpm, which is set by the 1 m length of the profiler. The upper wave number bound k_U is determined by an iterative procedure (Prandke and Stips (1998)). Assuming isotropy of the small-scale turbulence the dissipation rate ε was then estimated through:

$$\varepsilon = 7.5\,\nu\,\overline{(\partial_z u')^2}\ [m^2 s^{-3}] \tag{6}$$

Here, $\partial_z u'$ is the vertical profile of the current shear fluctuations and ν is the kinematic viscosity of water. The overbar denotes ensemble averaging, a theoretical procedure considering the mean value of an infinite number of realisations, see Lesieur (1997), which is here replaced by spatial/temporal averaging. Finally, the dissipation rate is corrected for the lost variance below and above the used integration limits and for the limited spatial response of the sensor.

A detailed discussion of the errors involved in the estimation of ε is found in Moum and Lueck (1985). The error estimate for this application is, that ε was determined within a factor of 2, when above 10^{-9} $m^2 s^{-3}$. The short

cable between profiler and buoyancy body, hanging below the profiler generated vibrations. Because these vibrations contaminated the spectra, the noise threshold was $3 \cdot 10^{-10}$ $m^2 s^{-3}$.

To avoid the calculation of unrealistic dissipation rates when the shear sensor is already in air, the determination of the exact point, when the sensors passes the surface is important. This transition point was automatically determined from the changing signal of a fast conductivity sensor, the fast thermistor and the typically very abrupt change within the shear signal. Afterwards each single profile was cut at that point, after manual inspection of the respective sensor signals. The uncertainty of the resulting surface point (zero depth), is better than ± 1 cm. The pressure signal was used to calculate the profiler velocity. As this signal is influenced by waves near the surface, a linear least square fit of the pressure data was done, assuming only first order changes in the uppermost 5 m.

3.4 Wind forcing

In order to get meteo data which reflect the atmospheric conditions of the open water, the meteorological station was moored about 2 km from the shore (figure 1). Wind velocities measured at 2.8 m above the water surface, were rescaled to the standard height of 10 m. During the microstructure data collection, the mean wind speed was 3.2 ms^{-1} at the meteo buoy. This rather low level was interrupted on two occasions, lasting for approximately one day, when the wind speed exceeded 6 ms^{-1} (figure 2). The first occasion was on March 10/11 and the second occasion on March 12/13, when the maximum wind gusts, recorded reached 14.6 ms^{-1} around midnight. Until March 14,

NNE-winds prevailed clearly ($\sim$ 73% of all wind direction measurements) indicating that the wind was parallel to the lake. Especially during the two main events, wind blew almost parallel to the longside of the lake and had subsequently a long fetch. After March 14, winds exceeding 4 ms^{-1} occurred as short pulses of less than one hour duration. Their directions were mainly from NNW and subsequently had short fetches. Therefore the most interesting period to look at will be the 4 days episode of March 10-13, when wind was high as well as variable and the fetch was long.

Wind speed was additionally measured by a small buoy about 50 m away from the microstructure probe locations with an anemometer at a height of 95 cm above the water surface. The accuracy is ± 0.1 m/s. This additional measurement allowed us to access the wind speed directly at the place of the dissipation rate sampling. Further we got evidence for the importance of frictional effects at the topography, which lead to a reduction of wind speed by 40% compared to the open lake values. Therefore we used this near-shore wind speed for simulating the dissipation rate data. Wind stress was calculated from wind speed using the Smith (1988) bulk formula and is presented in figure 2. Further, the individual wind events, with wind speed exceeding 3 m/s have been identified in figure 2 and table 3. The critical wind speed of 3 m/s was used, because we have seen, that at this wind speed first whitecaps occurred at the lake surface. For later reference each of these events is given a number which can be found together with the duration, mean wind stress and mean wind speed of the event in table 3. The duration of the identified event 6 was with less than 60 minutes rather short, but wind speeds between 2 and 3 m/s prevailed already some hours before it reached the threshold.

3.5 Surface waves

Surface waves were measured with a pressure transducer located 1.0 m below the surface and anchored at 40 m depth. Pressure was recorded at 4 Hz and with 1.5 cm resolution within a distance of about 100 m from the two microstructure profilers, see figure 1. From the time series of pressure, wave height spectra were calculated for ∼8 minutes long records and, after correcting for the installation depth (Bishop and Donelan (1987)), the significant wave height H_S [m] and the peak frequency f_p [s^{-1}] was calculated (Simon (1997)).

According to the wind direction, the maximum fetch was nearly half of the lake length and was therefore long enough to induce considerable wave height, see figure 3. Recorded wave heights reached a maximum of 0.66 m on March 10, shortly after wind reached its maximum. Two major wave events during March 10 and March 12 having $H_S > 20$ cm can be identified from the wave measurements, see lower bold lines in figure 3.

During the second half of the experiment, the wind blew in much shorter pulses (∼ hours), predominantly from north and west (i.e. from the shore) and with less directional persistence. As a result, the fetch and the pulses were too short to build up waves, which exceeded a significant wave height of 0.08 m (see figure 3). The peak frequency f_p varied between about 0.55 Hz for weak wind and 0.2 Hz for strong wind. These frequencies correspond to wave phase velocities between $c_p = g/(2\pi f_p) \approx$ 3 and 8 ms^{-1}. The corresponding wave numbers $k_p = (2\pi f_p)^2/g$ and wavelength $\lambda_p = 2\pi/k_p$ were between 1 m^{-1} and 0.14 m^{-1} and between 5 and 40 m, respectively.

Due to the wind action a small layer at the water surface will be accelerated and the resulting drift is named after its first investigator Stokes drift u_s (see Stokes (1847)). The Stokes drift decreases with depth as given by Skyllingstad and Denbo (1995):

$$u_s = (kH_S/2)^2 \sqrt{g/k}\, e^{-2kz} \tag{7}$$

Typical values for the stokes drift during the wind events at about 8 cm depth are between 2 and 7 cm/s, see table 4.

3.6 Heat Flux

Heatflux H_{net} was calculated from standard bulk formula (Henderson-Sellers (1986) and using the available shortwave measurements. H_{net} varied during the experiment between -340 and 750 Wm^{-2} with a mean heat input of $\sim$48 Wm^{-2}, see figure 4.

Until March 14, the mean temperature of the lake decreased during the nights with negative heat fluxes between -340 Wm^{-2} and -30 Wm^{-2}. Afterwards, with one exception at March 16 the net heat flux remained positive. The atmosphere just above the lake surface was usually unstable, as the air temperature at 2.8 m above the lake surface was lower than the water temperature during 73% of the time. Initially the experimental site was thermal stratified, but after the second wind event March 14 the water column was practically homotherm. Thermal stratification reestablished after March 15, see figure 5. The stability of the water column expressed as buoyancy frequency squared $N^2 = -(g/\rho)\partial\rho/\partial z \approx 10^{-5}\ s^{-2}$ was generally low as both the temperature

gradients and thermal expansivity α were small. Only in the top 3 m, N^2 exceeded $10^{-4}\ s^{-2}$. Below, the stability was less than $2 \cdot 10^{-5}\ s^{-2}$ until March 14. Afterwards, when wind generally ceased and the heat flux became positive (into the lake), stability increased throughout the SBL and N^2 reached $\sim 3 \cdot 10^{-5}\ s^{-2}$ for the bulk of the SBL.

3.7 Temperature field

The evolvement of the temperature field can be seen in figure 5. In the bulk of the water column the temperature was all the time between 5 and 6 ^oC. Only during short periods of sun shine the near surface layer reached temperatures above 6 ^oC, see the red spots in figure 5. Initial temperature stratification was mixed after wind event 1 March 10, reestablished March 11, but was destroyed during wind event 2, March 12. Even the contribution to mixing of the minor wind events 5 and 6 can be seen in figure 5. Still after March 15 the temperature stratification increased gradually until the end of the experiment. Following the storm during March 12/13 colder water of about 5.2 ^oC entered the measuring site. As this colder water was not produced by the local heat loss, it must have been advected to the measurement place.

3.8 Dissipation of turbulent kinetic energy

During the course of the experiment, turbulence was dominated by wind, as the surface buoyancy flux was small. During the two periods of strong cooling at March 10 and 12, wind was especially heavy and therefore exceeded the surface buoyancy flux which averaged at $\sim 1 \cdot 10^{-8}\ m^2 s^{-3}$ that night. In section

5 is is shown that production of TKE due to wind/wave forcing during the strong wind events was up to about 3 orders of magnitude larger than TKE production due to the surface buoyancy flux. The measured dissipation values varied over 5 orders of magnitudes from $\varepsilon \sim 10^{-10}$ to $\varepsilon \sim 10^{-5}\ m^2 s^{-3}$ and averaged at $\sim 2 \cdot 10^{-8}\ m^2 s^{-3}$ over the top 30 m. Within the usual scatter due to intermittency, dissipation followed the wind forcing, see section 4. Further, as a function of depth, dissipation resembled *law-of-the-wall* scaling, which means $\varepsilon \sim z^{-1}$. This will be discussed in more detail later.

4 Comparison of measured and simulated data

In this section we will compare the results from the observations with the performed simulations.

In order to assess the importance of advection and wave breaking for the experiment, different runs were performed. Run r1 applied the unmodified $k-\varepsilon$ model without wave breaking parameterisation and without relaxation of temperature. As this run did not give a realistic simulation, results from this run will not be considered further. As our aim is not to reproduce the dynamic of the temperature field, but we rather focus on the near surface turbulence, we decided to relax the simulated temperature field to the measured temperature profiles. Therefore again the unmodified $k-\varepsilon$ model was used for run r2, but in this case the simulated temperature was relaxed to the measured. In run r3 the Craig/Banner wave parameterisation was activated. Additional for run r4 the surface roughness length z_0 was increased by a factor of 10. Different sensitivity tests were done, which will be only briefly mentioned, when necessary.

4.1 Dissipation rate field

Observed and simulated dissipation rates (run r2) in the depth interval 30 to 0 m are shown in figure 6. From this figure 6 we see that all the major and minor wind events during the experiment lead to enhanced near surface dissipation rates in the measurements, as well as in the simulated ε. During the major wind events increased dissipation rates can be found as deep as the measurements were done (32 m), but even the minor wind events show higher dissipation rates down to about 20 m. Run r2 shows an acceptable

simulation, as the higher dissipation rates produced at the surface during the major wind events are extending down to the bottom in accordance with the measurements. Still, especially during the minor wind events the higher levels of observed dissipation rates reach deeper than in the simulations. Further, the model needs much more time to increase dissipation at about 30 m. This is likely due to the additional effect of vertical convection during the nocturnal cooling, which results in a downgradient flux of TKE. This convective flux is only to first order parameterised within GOTM, see Stips et al. (2002) and therefore cannot be well reproduced. The small-scale variability in the measurements is higher than in the simulation. This is caused by the intermittency in the measurements, which is excluded in the used type of turbulence model. Run r3 and run r4 would not show evident differences to run r2 in this overview plot and are therefore not shown. Therefore we are forced to look into the details at the near surface to see possible effects of wave breaking.

4.2 Time series of dissipation rate

The time series of the averaged near surface dissipation rate in the uppermost meter is shown in figure 7. The simulated near surface dissipation rates, without consideration of wave breaking (run r2), underestimates the measured ones during most of time quite considerable. Applying the wave breaking parameterisation (run r3), most of the wind events are reproduced rather well.

Very well reproduced are the major wind event 2 and the minor wind events 5 and 6. The performed simulation of the wind events 1, 3 and 4 match less well with the data. Wind event 3 has rather specific characteristics as the wind is decreasing and changing direction from NE to NW, but on the other hand

there are still larger waves present. Practically the opposite happened during wind event 1, where the wind was increasing, but changed direction from NW to NE during the event. During March 13, when the wind was decaying, observed dissipation rate exceeds all simulations nearly at all times. On most other occasions observed ε responded with a quick decrease to decaying wind, as e.g. on March 11, 14, 15, 17 and 19. This different behaviour of ε cannot be explained from the available data.

Looking only at the wind events, we can suspect, that the well simulated wind events are characterised by a wind having rather constant magnitude and direction. The improvement due to an increased surface roughness length (run r4), can be hardly identified on the scale of this plot. Only during very limited time periods, the black line from run r3 can be identified at lower levels compared to run r4 (red line). The influence of the duration of the wind seems not so clear, as e.g. wind event 4 and 5 have similar duration, the wind is coming from the same direction, but only event 5 is very well reproduced.

Analysing the correlation between the logarithm of the measured and simulated surface dissipation rates (see table 5), we find a slightly better correlation for runs r4 and r3 compared to run r2. Further the slope of the linear regression curve approaches more closely the ideal slope of 1.

4.3 Near surface slope of dissipation rate

The near surface slope of the dissipation rate, averaged over the duration of the different identified wind events, is shown in figure 8. The black circles are the results from the simulation without (r2), black dots are with considera-

tion of wave breaking (r3) and the red dots are from run r4 with increased surface roughness length. The blue dots are mean values calculated from the measured data. In all 6 cases there is a clear improvement of the simulated dissipation rate using the wave breaking parameterisation (r3) compared to the unmodified $k-\varepsilon$ model (r2). The major wind events 1 and 2 are even better reproduced, when using an increased surface roughness length, as done for run r4. The influence of this increased z_0 on the minor wind events is minimal. As a side effect the influence of the different window length on the avearge of the measured data becomes evident from figure 8. The decreasing averaging time from event 1 and 2 (around 18 hours) to event 3 and 4 (around 3 hours) and down to finally event 5 and 6 (around 1 hour) leads to a much higher variability in the depth range below 1 m. Further it is demonstrated that already at such rather low wind speeds a clear signal from sporadic breaking events is evident. In the depth range above about 1 m to 0.5 m the simulated values from run r3 as well as the measured data deviate from the classical LOW slope of z^{-1}, which is represented by the open circles from run r2. The slope of ε in the uppermost 1 m was calculated using a least square fit for the decadal logarithm of ε with depth. The respective values found for the wind events are given in table 6. Of course the unmodified $k-\varepsilon$ model (run r2) leads to the expected slope of about z^{-1}. The improved model with including wave-breaking (run r3), gives near surface slopes of around $z^{-1.7}$, where as the measured longer wind events have a slope of about $z^{-1.9}$. The correlation coefficient is in all investigated cases around 0.99 (not shown), which clearly confirms the very good fit and that it is correct to use a linear regression model. The depth of the WASL is likely to be depending on the wind speed and wave height. The depth of a significant increased ε is 1.3 m, 1.5 m and 0.6 m for wind event 1, 2 and 3 respectively (figure 8). This could be explained

to be either about $3 * H_S$ or could be calculated from a product of wind speed and wave height (to be scaled in order to get the correct dimension). As we have too few points for an extended analysis, we are not able to provide a definitive statement on this matter.

In the case of the 2 major wind events the measured uppermost ε value could fall in the depth of the wave-turbulent sublayer and would therefore scale different. There is indeed some indication that the measured uppermost ε does not continue the slope of the deeper values.

The major wind events 1 and 2 show also in the depth range below 1.5 m slightly increased dissipation rates. This is likely to be caused by higher order transport processes, which are not parameterised in the second order $k - \varepsilon$ scheme. Only a model which also considers the third-order moments, like that described in Canuto et al. (1994) could be capable of reproducing such features.

5 Discussion

5.1 General features of the simulations

In early March, the temperature stratification was very weak and temporal changes were dominated by advection of lateral inhomogeneties. It is clearly not the scope of the present paper to perform a 3D simulation on the investigated lake. Therefore the performed relaxation of the simulated temperature field to the measured temperatures represents a compromise between the sufficient accurate reproduction of the experimental data and the needed effort. Only with applying relaxation of temperature (run r2) the simulated dissipation rate showed a similar dynamics as the measured, see figure 6. Still during most of the time the standard $k-\varepsilon$ model, especially near the surface (within the uppermost meter) underestimates the dissipation rates by up to 1 order of magnitude, see figure 7. Considering the prevailing light to moderate wind conditions of maximal only about 8 m/s at the profiler site, this might come as a surprise. By visual observations we could see first white caps as an indice for wave breaking already starting at around 3 m/s. Therefore using the wave breaking parameterization as proposed by Craig and Banner (1994) and incorporated in the $k-\varepsilon$ model by Burchard (2001b) certainly improved the simulation, as could be seen in figure 7. Still we found that the near surface ε values are underestimated, in the case of the major wind events.

5.2 Scaling of near surface dissipation rate

Applying appropriate scaling, near surface dissipation rates under breaking waves should collapse more or less into one curve, see Terray et al. (1999). In the non-breaking case the near surface dissipation rate is usually made nondimensional by applying the factor $1/(u_*^3/z_0)$ according to the LOW (Lombardo and Gregg (1989), whereas the nondimensional depth $\tilde{z}$ will become $(z_0 - z)/z_0$. Here we are using a surface roughness length calculated according to the Charnok formula, see equation 5. When wave-breaking is important the depth will be scaled by the significant wave heigth H_S instead, so that $\tilde{z} = (z_0 - z)/H_s$. The nondimensional dissipation rate $\tilde{\varepsilon}$ will be defined as $\varepsilon/(c_w u_*^3/H_s)$, with $c_w = 100$ for all considered wind events. We can use a constant wave breaking parameter c_w here, as the increasing probability of wave breaking with increasing wind speed is somehow already represented by the appearance of u_*^3 in the scaling law.

In figure 9 data and model results from this study are compared to published observations in the WASL by Terray et al. (1999), Drennan et al. (1996) and Anis and Moum (1995). The slope in our data is slightly smaller than that from the other measurements. The applied scaling works for most of the data from event 1, 2 and event 3 rather well, as the points fall practically on one line. An exception is the uppermost point for both major events, which does not follow that line. This point would however fit well, if we would assume that the respective dissipation rate was underestimated by a factor of 3. On the other hand there is some speculation about the existence of a thin wave-turbulent layer of constant ε with thickness z_0 directly at the surface (Burchard (2001b)). This would be supported by the existence of this point, which appears to be

scaled too small. For weaker wind and waves such a near surface outlier is not existing, a fact which is further supporting this speculation. The three sets of near surface dissipation rates from the literature, were scaled by Terray et al. (1999) using the significant wave height H_S. The ratio of z_0/H_S for these data is 0.85. Using z_0 values derived from the Charnok formula (equation 5) as for run r2 we find z_0/H_S ratios of 0.012 and 0.022 for event 1 and 2 respectively. With such a low ratio the model underestimates the measured data. By far better is $10 * z_0/H_S$, the ratio used for run r4, being 0.12 and 0.22 for event 1 and 2. Therefore, in accordance with Gemmrich and Farmer (1999), we would reject the assumption of a fixed z_0/H_S ratio as done by Terray et al. (1999) and certainly their value of 0.85 seems far too large.

5.3 Surface roughness length

The determination of an appropriate surface roughness length seems to be the major problem for applying the new theory, as this input parameter must be provided a priori (from the measurements). Several authors (see Craig and Banner (1994), Terray et al. (1996), Drennan et al. (1996), Gemmrich and Farmer (1999)) had proposed that the relevant length scale at the surface in the case of wave-breaking will not be surface roughness length of a classical wall layer. Terray et al. (1996) and Drennan et al. (1996) proposed the significant wave height as relevant length scale, but this was contradicted by Gemmrich and Farmer (1999).

We investigated the influence of different chosen z_0 on the simulations, especially on the fit in the WASL. When using GOTM, the simplest way for doing so is to change the coefficient α of the Charnok (1955) formula. Instead of the

standard $\alpha = 1400$ (Craig and Banner (1994)) we used also values of 5600, 14000 and 56000. Then the resulting maximal z_0 for a wind speed of 5 ms^{-1} will be about 0.02 m, 0.05 m and 0.2 m respectivly instead of 0.005 m for the standard value. Only when using $\alpha = 14000$ the simulations agree rather well with the observations. The value of 5600 gives similar results as run r3 using the standard value and the largest value (56000) leads to an unrealistic overestimation of the near surface dissipation. Enhanced dissipation rates extend to much greater depth then observed ones. Therefore we must conclude that at least for such small wind speeds as persisted during our experiment z_0 is larger than usually assumed, but still much smaller than the significant wave height H_S. This finding seems to contradict Terray et al. (1996), as they found that an appropriate z_0 would be in the order of H_S (Terray et al. (1996),Drennan et al. (1996), Craig (1996)). Field measurements by Gemmrich and Farmer (1999) showed a much smaller z_0 and a different relation between significant wave heigt and surface roughness length. Gemmrich and Farmer (1999) found a z_0 of about 0.2 m for wind speeds of $U_{10} = 15\ ms^{-1}$. Applying this increased coefficient in the Charnok formulation (see equation 8), would result in $z_0 \approx 0.165\ m$ for a wind speed of 15 ms^{-1}. A wind speed of $U_{10} = 25\ ms^{-1}$ would give a z_0 of 0.29 m. Therefore our results clearly support the view of a smaller surface roughness length, but still larger than the conventionell assumed, which would be defined in the following way:

$$z_0^{new} = 14000\, u_*^2/g \tag{8}$$

The uppermost point from the windevents 1 and 2 fall outside the applied scaling, see figure 9. This could be a sign for the postulated layer of constant

dissipation rate,as these values are representative for a depth of 0.075 m and therefore fall within in the depth range of the postulated breaking zone as found by Terray et al. (1996) $z_b \approx 0.6 H_S$. The next deeper value is at about 0.015 m depth would still fall within this depth range, but in our data it follows already the proposed scaling with wind and wave forcing. Therefore also this seems to support the view of a much shallower breaking zone in the order of z_0 only. The transition to the classical wall layer seems to appear at about a depth of 2-3 times the significant wave heigth.

5.4 TKE budget

An interesting question is, what are the contributions to the TKE production from shear, buoyancy and wave breaking during the identified wind events. Therefore we integrated dissipation rate, shear production P_S and buoyancy production P_B over the uppermost meter for the 6 identified wind events. The first obvious result is, that the contribution from buoyancy production P_B is negligible, as can be seen from the results presented in table 7. We therefore do not consider further buoyancy production in this discussion. For run r2 the TKE production is not shown, but as the above mentioned balance is incorporated in the k-ε model, the respective values are nearly identical to the dissipation rates. Simulated ε increased in run r3 by a factor of 2.5 compared to run r2, whereas P_S increased by a factor of 2. For run r3 shear production P_S is for all wind events about 80 % of the respective dissipation rate. The simulated ε is again increased for run r4, now by a varying factor between 3 to 6 compared to run r2. The opposite is happening to P_S, which is now smaller than the values for run r3 and in the case of wind event 2 even

smaller than that from run r2. This is related to the fact, that in this case TKE production in the near surface zone is mainly caused by wave breaking instead of shear production. The event 2, which had the strongest wind seems to be best simulated, as ε from run r4 and from the data agree rather well. In the case of the other two events with larger waves (1,3) the measured dissipation is exceeding the simulated dissipation by approximately a factor of 2. Only in the case of the minor wind events 4 and 6, simulated dissipation is larger than the measured one. From these results it is obvious that near surface ε will be only simulated in the correct order of magnitude, when the TKE production due to breaking waves is taken into account.

We would like to further quantify the contributions to TKE production from the energy of breaking waves by using a simple linear model and from the Stokes drift in order to estimate the importance of these processes. The linear model assumes that the rate of TKE production due to breaking waves P_{wave} is proportional to the wave energy content E_W multiplied by some inverse dissipation time scale of the wave energy (Longuet-Higgins (1969)):

$$P_{wave} = 1600 C_D^{3/2} \frac{\rho_{Air}}{\rho} f_p E_W \ [Wm^{-2}] \tag{9}$$

where C_D is the drag coefficient, f_p is the peak frequency (see table 4) and ρ is density. The resulting values from this linear model P_{wave} (see table 8) are always much smaller than the measured dissipation rate. For event 1 P_{wave} exceeds the simulated ε from run r3, but is lower than that from run r4. For the other two events with waves 2 and 3 this linear estimate is below ε from run r3. Therefore it is evident, that the linear wave breaking model alone cannot explain the measured near surface ε.

A different estimation for the surface flux of TKE due to breaking waves was proposed in Terray et al. (1996) and in Gemmrich and Farmer (1999)

$$P_{breaking} = \overline{c_P}\,\rho\,u_*^2\ [Wm^{-2}] \tag{10}$$

where u_* is the friction velocity in water, ρ is density and $\overline{c_P}$ is the effective phase speed of waves acquiring energy from the wind. Using $\overline{c_P} \approx 0.1 c_P$ (Terray et al. (1996), table 4) we will get values between 10 to 29 mWm^{-2}, see table 8. These estimates exceed all other estimates and the measured turbulent dissipation rates. For the events 1, 2 and 3 $P_{breaking}$ is between 20 to 70 % above the measured ε, so they are larger, but not a different order of magnitude. Taking into account that the waves at lake Neuchâtel are young waves, then $\overline{c_P}$ should be even larger, which would result in even larger estimates.

The interaction of the vortex force associated with the Stokes drift u_s (see Stokes (1847)) and the current shear in the presence of Langmuir circulation could be another potential source of TKE production (Skyllingstad and Denbo (1995)). The production P_{Stokes} is then defined by:

$$P_{Stokes} = \tau\,u_S\ [Wm^{-2}] \tag{11}$$

with u_S as defined in equation 7. Because of the exponential decay with depth of the Stokes drift, this related production will be confined to thin near surface layer, which scale with the inverse of the wavenumber k. In table 8 it can be seen, that in the case of existing waves the related TKE production P_{Stokes} is of similar importance as the shear production or the production due to wave breaking estimated from the linear model. The contribution from wave

breaking as simulated by the k-ε model is given in column 2 of table 8 ($\varepsilon - P_S$). For event 1 and 3 this is similar to P_{wave}, but for event 2 it is a factor of 7 larger. As this is opposite to the ε simulation, it seems that TKE production due to wave breaking is not well quantified yet.

It can be concluded that in the case of wind speeds above 3 m/s, but without corresponding wave development all energy estimates only based on wave parameters seem to fail. If similar wind speeds are accompanied by waves with significant wave heights of above 20 cm these estimates give some first order approximation of the TKE production due to breaking waves, but the linear model and Stokes drift give too small values, whereas equation 10 gives too large values.

5.5 Intermittency

Wave breaking is a very intermittent process, therefore also the related turbulence levels are supposed to be very intermittent. Phillips (1985) showed theoretically that breaking frequency and whitecap coverage should be proportional to u_*^3. It is likely that the measured mean turbulence level is orders of magnitude smaller than the level which occurred directly after a breaking event. Rapp and Melville (1990) estimated the temporal decay of of dissipation rate ε beneath breaking laboratory waves, and found that $\varepsilon \propto t^{-5/2}$.

Gemmrich (2000) states that for timescales comparable to the period of breaking waves, advection due to Langmuir circulation can be neglected. The time between successive breaking events at wind speeds between 3 - 6 m/s is O(600 s), The duration of breaking events is in the order of 0.5 to 3 s (see

Gemmrich (2000), Eifler and Donlon (2001)).

Considering this low breaking frequency, the short duration of the breaking events and the fast decay time of dissipation after the breaking event, we must ask ourself, can we measure enhanced near surface dissipation rates due to wave breaking using vertical profiler snap shots? As we measured indeed increased near surface dissipation, there remain two possibilities, the first is that the decay time is much longer than usually assumed or the second being that we do not measure breaking events, but interaction of Stokes drift and Langmuir circulation. Gemmrich (2000) concludes from his measurements that the decay time is very short (less 20-30 s), which would point to the second option. On the other hand the energy considerations from subsection 5.4 gave far too small values for the TKE production due to these nonlinear processes. Therefore we are not able to exclude one or the other possibility with certainty.

6 Summary and conclusions

Two major questions had to be examined in this paper, the first do we measure enhanced dissipation in the wave affected layer at wind speeds below 8 ms^{-1} using a vertical profiler and the second can we simulate this wave affected layer with current days turbulence models.

As could be shown in the previous sections, we find a layer of increased turbulence compared to the *law-of-the-wall* near to the surface. Therefore the first question can be answered positively, also with vertical profiling instruments the enhanced turbulence in the wave affected layer can be measured successfully. The profiling method is especially beneficial for completely assessing the topmost 1 m layer. We found the near surface slope of ε to be $\approx$ -2.0 in the case of wind speeds above 4 ms^{-1}. Further our high resolution near surface measurements of dissipation rate show already at wind speeds above about 2 ms^{-1} clear evidence of a wave affected layer with increased ε compared to the classical *law-of-the-wall*, having a thickness between 0.1 and 1.2 m. In terms of the significant wave height H_S this wave affected layer reached to a depth of about 2 to 3 * H_S. This indeed provokes the question, if really only wave breaking could be the cause of this enhanced dissipation, or would there be other processes of importance, as the interaction of the current shear from Langmuir circulation with that from the Stokes drift. That we found already enhanced dissipation at rather low speeds, where breaking events are unlikely to occur gives some evidence to the assumption that these enhanced ε are not only caused by wave breaking. This question cannot be answered finally in the frame of the present work, but should be addressed with specific measurement setups.

The other major challenge for writing this paper was, to test if this wave affected layer can be reproduced by current day turbulence models. Here we could demonstrate that TKE dissipation rates in the near surface region were realistically simulated using the 1D k-ε turbulence closure (GOTM), when the effects of wave breaking on turbulence production are considered, as proposed by Burchard (2001b). This is true with regard to the magnitude of the near surface dissipation, as well as the depth range of the increased ε and the exponential decay of ε away from the surface, showing a power law of about $z^{-1.9}$.

Obviously one of the major problems for successful simulating near surface turbulence is not directly related to the modelling itself, but how to find proper values for the surface roughness length, as the most critical model input parameter. Only when increasing the surface roughness length z_0 calculated from the Charnok formula by a factor of 10, the dissipation rate in the wave affected layer could be realistically simulated. Therefore it seems also that we are still missing some basic physical understanding of the meaning of the roughness length in the case of breaking waves. We could not confirm that z_0 would scale with the significant wave height as assumed by Drennan et al. (1996). The best fit to our data, if scaled to a wind of 15 ms^{-1}, would result in z_0 values of similar magnitude as reported by Gemmrich and Farmer (1999), but seems still to be about 20% smaller then his data.

In summary our results clearly support the view of a smaller surface roughness length as proposed by Craig and Banner (1994) or Drennan et al. (1996), but still much larger than the conventionell assumed. Care should be taken that the wave affected layer showing increased dissipation rates in the depth range of order of 1 to 3 * H_S is not confused with the surface roughness length. The

measurements further indicate, that an assumed wave breaking zone having a constant dissipation rate would exist only in the depth range of the increased z_0 (1-20 cm).

Future work should be directed to measurements, that would allow to separate shear generated turbulence production from turbulence generated by wave breaking (no shear), in order to clarify the contributions from each part to the near surface production. But most importantly work must be carried out to determine the surface roughness length (or surface mixing length as proposed by Gemmrich and Farmer (1999)) as a function of wind and wave parameters. This should also clarify if really a layer of constant ε is existing near to the surface.

Acknowledgement: Performing this extensive measurement campaign was only possible with the help of several colleagues from the Environmental Physics department at EAWAG and the Inland and Marine Waters Unit of JRC. Thanks to all of them, but especially to Andre Simon, Otti Kocsis, Michael Schurter, Ulisse Devisioni, Bjarke Rasmussen and Alexander Pufahl. Ute Stips volunteered to reprocess the shear data and made the quality control of the dissipation rate data.

7 Appendix

Here, it is briefly demonstrated how some of the empirical parameters for the extended k-ε model are calculated. This extends the algebra contained in Burchard (2001a) which was shown for the standard k-ε model with constant c_μ, only. Here, the stability functions of Canuto et al. (2001) with shear-dependence are used. The stability function for LOW conditions is calculated by means of $P + B = \varepsilon$ which is equivalent to

$$c_\mu(\alpha_M, \alpha_N)\alpha_M - c'_\mu(\alpha_M, \alpha_N)\alpha_N = 1 \tag{12}$$

with the stability functions c_μ and c'_μ for momentum and tracers, respectively, the shear and buoyancy parameters, $\alpha_M = M^2k^2/\varepsilon^2$ and $\alpha_N = N^2k^2/\varepsilon^2$, respectively, and the shear squared, $M^2 = (\partial_z u)^2 + (\partial_z v)^2$ and the Brunt-Väisälä frequency squared, $N^2 = -(g/\rho_0)\partial_z\rho$. The numerical solution of the implicit function for $\alpha_N = 0$ is $c_\mu = 0.07715$. For shear-free turbulence with $P/\varepsilon = 0$ and thus $\alpha_M = \alpha_N = 0$ we computed directly from the definition of the Canuto et al. (2001) stability functions that $c_\mu = 0.107$. With the other

parameters given in table 1, the equations (14), (16) and (17) in Burchard (2001a) compute directly $m = 2.238$, $\sigma_{\varepsilon,LOW} = 1.2$ and $\sigma_{\varepsilon,WASL} = 2.012$.

References

Agrawal, Y. C., Terray, E. A., Donelan, M. A., Hwang, P. A., Williams III, A. J., Drennan, W. M., Kahma, K. K., Kitaigorodskii, S. A., 1992. Enhanced dissipation of kinetic energy beneath surface waves. Nature 359, 219–220.

Anis, A., Moum, J. N., 1992. The superadiabatic surface layer of the ocean during convection. J. Phys. Oceanogr. 22, 1221–1227.

Anis, A., Moum, J. N., 1995. Surface wave-turbulence interactions: Scaling $\varepsilon(z)$ near the sea surface. J. Phys. Oceanogr. 25, 2025–2045.

Benilov, A. Y., Ly, L. N., 2002. Modelling of surface waves breaking effects in the ocean upper layer. Math. and Comp. Model 35, 191–213.

Bishop, C. T., Donelan, M. A., 1987. Measuring waves with pressure transducers. Coastal Engineering 11, 309–328.

Burchard, H., 2001a. On the q^2l equation by Mellor and Yamada [1982]. J. Phys. Oceanogr. 31, 1377–1387.

Burchard, H., 2001b. Simulating the wave-enhanced layer under breaking surface waves with two-equation turbulence models. J. Phys. Oceanogr. 31, 3133–3145.

Burchard, H., 2002. Applied turbulence modelling in marine waters. Vol. 100 of Lecture Notes in Earth Sciences. Springer, Berlin, Heidelberg, New York.

Burchard, H., Baumert, H., 1995. On the performance of a mixed-layer model based on the k-ε turbulence closure. J. Geophys. Res. 100, 8523–8540.

Burchard, H., Bolding, K., 2002. GETM, a general estuarine transport model. Scientific documentation. Tech. Rep. EUR 20253, European Commsission,

Ispra.

Burchard, H., Bolding, K., Ruiz-Villarreal, M., 1999. GOTM – a general ocean turbulence model. Theory, applications and test cases. Tech. Rep. EUR 18745 EN, European Commission.

Burchard, H., Deleersnijder, E., 2001. Stability of algebraic non-equilibrium second-order closure models. Ocean Modelling 3, 33–50.

Burchard, H., Stips, A., Eifler, W., Bolding, K., Villarreal, M. R., 2000. Numerical simulation of dissipation measurements in non-stratified and strongly stratified estuaries. In: Yanagi, T. (Ed.), Interactions between estuaries, coastal seas and shelf seas. Terra Scientific Publishing, Tokyo, pp. 1–18.

Businger, J. A., Wyngaard, J. C., Izumi, Y., Bradley, E. F., 1971. Flux profile relationships in the atmospheric surface layer. Journal of Atmospheric Sciences 28, 181–189.

Canuto, V. M., Howard, A., Cheng, Y., Dubovikov, M. S., 2001. Ocean turbulence. Part I: One-point closure model - Momentum and heat vertical diffusivities. J. Phys. Oceanogr. 31, 1413–1426.

Canuto, V. M., Minotti, F., Ronchi, C., Ypma, M., Zeman, O., 1994. Second-order closure PBL model with new third-order moments: Comparison with LES data. Journal of Atmospheric Sciences 51, 1605–1618.

Charnok, H., 1955. Wind stress on a water surface. Q. J. R. Meteorol. Soc. 81, 639–640.

Craig, P. D., 1996. Velocity profiles and surface roughness under breaking waves. J. Geophys. Res. 101, 1265–1277.

Craig, P. D., Banner, M. L., 1994. Modelling wave-enhanced turbulence in the ocean surface layer. J. Phys. Oceanogr. 24, 2546–2559.

Dillon, T. M., Richman, J. G., Hansen, C. G., Pearson, M. D., 1981. Near-surface turbulence measurements in a lake. Nature 290, 390–392.

Donelan, M. A., 1998. Air-water exchange processes. In: Imberger, J. (Ed.), Physical processes in lakes and oceans. Vol. 54 of Coastal and Estuarine Studies. pp. 19–36.

Drennan, W. M., Donelan, A. A., Terray, E. A., Katsaros, K. B., 1996. Oceanic turbulence dissipation rate measurements in SWADE. J. Phys. Oceanogr. 26, 808–815.

Eifler, W., Donlon, C. J., 2001. Modeling the thermal surface signature of breaking waves. J. Geophys. Res. 106, 27163–27185.

Gemmrich, J. R., 2000. Temperature anomalies beneath breaking waves and the decay of wave-induced turbulence. J. Geophys. Res. 105, 8727–8736.

Gemmrich, J. R., Farmer, D. M., 1999. Near-surface turbulence and thermal structure in a wind-driven sea. J. Phys. Oceanogr. 29, 480–499.

Gemmrich, J. R., Farmer, D. M., 2004. Near-surface turbulence in the presence of breaking waves. J. Phys. Oceanogr.In print.

Gibson, C. H., 1982. Alternative interpretations for microstructure patches in the thermocline. J. Phys. Oceanogr. 12, 374–383.

Henderson-Sellers, B., 1986. Calculating the surface energy balance for lake and reservoir modeling: A review. Reviews of Geophysics 24, 625–649.

Kantha, L. H., Clayson, C. A., 2004. On the effect of surface gravity waves on mixing in the oceanic mixed layer. Ocean Modelling 6, 101–124.

Kitaigorodskii, S. A., Donelan, M. A., Lumley, J. L., Terray, E. A., 1983. Wave turbulence interactions in the upper ocean. Part II: Statistical characteristics of wave and turbulent components of the random velocity field in the marine surface layer. J. Phys. Oceanogr. 13, 1988–1999.

Kocsis, O., Prandke, H., Stips, A., Simon, A., Wüest, A., 1999. Comparison of dissipation of turbulent kinetic energy determined from shear and temperature microstructure. J. Mar. Sys. 21, 67–84.

Lass, H. U., Prandke, H., 2003. A study on the turbulent mixed layer in the Baltic Sea. In: Chmielewski, F. M., Foken, T. (Eds.), Beiträge zur Klima- und Meeresforschung. Berlin, Bayreuth, pp. 159–168.

Lesieur, M., 1997. Turbulence in fluids, 3rd Edition. Vol. 40 of Fluid mechanics and its applications. Kluwer Academic Publ., Dordrecht.

Lombardo, C. P., Gregg, M. C., 1989. Similarity scaling of viscous and thermal dissipation in a convecting surface boundary layer. J. Geophys. Res. 94, 6273–6284.

Longuet-Higgins, M., 1969. On wave breaking and the equilibrium range of wind-generated waves. Proc. Roy. Soc. London A310, 151–159.

Lorke, A., Wüest, A., 2002. Probability density of displacement and overturning length scales under diverse stratification. J. Geophys. Res. 107, 3214–3225, doi:10.1029/2001JC001154.

Mellor, G. L., Yamada, T., 1974. A hierarchy of turbulence closure models for planetary boundary layers. Journal of Atmospheric Sciences 31, 1791–1806.

Mellor, G. L., Yamada, T., 1982. Development of a turbulence closure model for geophysical fluid problems. Rev. Geophys. 20, 851–875.

Monin, A. S., Obukhov, A. M., 1954. Basic laws of turbulent mixing in the ground layer of the atmosphere. Akad. Nauk SSSR Geofiz. Inst. Tr. 151, 163–187.

Moum, J. N., Lueck, R. G., 1985. Causes and implications of noise in oceanic dissipation measurements. Deep-Sea Research 32, 379–390.

Osborn, T. R., Farmer, D. M., Vagle, S., Thorpe, S. A., Cure, M., 1992. Measurements of bubble plumes and turbulence from a submarine. Atmos.-Ocean 30, 419–440.

Phillips, O. M., 1985. Spectral and statistical properties of the equilibrium range in wind-generated gravity waves. J. Fluid Mech. 156, 505–531.

Prandke, H., Stips, A., 1998. Test measurements with an operational microstructure-turbulence profiler: Detection limit of dissipation rates. Aquatic Sciences 60, 191–209.

Rapp, R. J., Melville, W. K., 1990. Laboratory measurements of deep-water breaking waves. Phil. Trans. R. Soc. Lond. A 331, 731–800.

Rodi, W., 1980. Turbulence models and their application in hydraulics. Tech. rep., Int. Assoc. for Hydraul. Res., Delft, The Netherlands.

Sander, J., Simon, A., Jonas, T., Wüest, A., 2000. Surface turbulence in natural waters: A comparison of large eddy simulations with microstructure observations. J. Geophys. Res. 105, 1195–1207.

Simon, A., 1997. Turbulent mixing in the surface boundary layer of lakes. Ph.D. thesis, Swiss Federal Institute of Technology, Zürich, Switzerland, diss. ETH No. 12272.

Simpson, J. H., Burchard, H., Fisher, N. R., Rippeth, T. P., 2002. The semi-diurnal cycle of dissipation in a ROFI: model-measurement comparisons. Cont. Shelf Res. 22, 1615–1628.

Skyllingstad, E. D., Denbo, D. W., 1995. An ocean large-eddy simulation of Langmuir circulations and convection in the surface mixed layer. J. Geophys. Res. 100, 8501–8522.

Smith, S. D., 1988. Coefficients for sea surface wind stress, heat flux, and wind profiles as a function of wind speed and temperature. J. Geophys. Res. 93, 15467–15472.

Stips, A., Burchard, H., Bolding, K., Eifler, W., 2002. Modelling of convective turbulence with a two-equation k-ε turbulence closure scheme. Ocean Dynamics 52, 153–168.

Stips, A., Prandke, H., 2000. Recommended algorithm for dissipation rate calculation within PROVESS. Tech. Rep. I.00.116, European Commission,

Joint Research Centre, Ispra, Italy.

Stokes, G. G., 1847. On the theory of oscillatory waves. Trans. Camb. Phil. Soc. 8, 441–455.

Terray, E. A., Donelan, M. A., Agrawal, Y. C., Drennan, W. M., Kahma, K. K., Williams III, A. J., Hwang, P. A., Kitaigorodskii, S. A., 1996. Estimates of kinetic energy dissipation under breaking waves. J. Phys. Oceanogr. 26, 792–807.

Terray, E. A., Drennan, W. M., Donelan, M. A., 1999. The vertical structure of shear and dissipation in the ocean surface layer. In: Banner, M. L. (Ed.), The wind-driven air-sea interface-electromagnetic and acoustic sensing, wave dynamics and turbulent fluxes. pp. 239–245.

Thorpe, S. A., 1977. Turbulence and mixing in a Scottish loch. Phil. Trans. R. Soc. Lond. A 286, 125–181.

Thorpe, S. A., Osborn, T. R., Jackson, J. F. E., Hall, A. J., Lueck, R. G., 2003. Measurements of turbulence in the upper-ocean mixing layer using autosub. J. Phys. Oceanogr. 33, 122–145.

Umlauf, L., Burchard, H., 2003. A generic length-scale equation for geophysical turbulence models. Journal Marine Research 61, 235–265.

Umlauf, L., Burchard, H., Bolding, K., 2004. General Ocean Turbulence Model. Source code documentation. Tech. rep., Baltic Sea Research Institute Warnemünde, Warnemünde, Germany, in print.

Zhang, K. Q., Chan, E. S., 2003. Modeling of the turbulence in the water column under breaking wind waves. Journal of Oceanography 59, 331–341.

8 Tables

σ_k	$\sigma_{\varepsilon,LOW}$	$\sigma_{\varepsilon,WASL}$	c_1	c_2	$c_3,\ N^2 > 0$	$c_3,\ N^2 < 0$	κ	c_w
1.0	1.2	2.01	1.44	1.92	-0.629	1.0	0.4	100

Table 1
Empirical constants for the extended k-ε model by Burchard (2001a) with the Canuto et al. (2001) second-moment closure.

Sensor	Longitude	Latitude	Denomination
Currentmeter 5 m	6^0 47'26.7	$46^0$53'51.6"	st
Currentmeter profiling	6^0 47'19.0"	$46^0$53'48.5"	sp
Currentmeter surface	6^0 47'17.0"	$46^0$53'55.9"	so
Microstructure temperature	6^0 47'23.2"	$46^0$53'54.2"	sw
Microstructure shear	6^0 47'23.0"	$46^0$53'53.1"	mi
Wave gauge	6^0 47'23.2"	$46^0$53'56.4"	Wb
Wind buoy	6^0 47'19.0"	$46^0$53'58.6"	Wi
Meteo buoy	6^0 47'38.4"	$46^0$53'32.6"	Me
Thermistors string	6^0 47'48.5"	$46^0$53'22.2"	tl

Table 2
Location and denomination of the moorings in figure 1 during the Lake Neuchâtel field experiment 1996.

Event	Start	End	Duration	Stress	Speed
-	UTC	UTC	hours	N/m^2	m/s
1	10.3472	11.0472	16.80	0.039	3.81
2	12.2069	13.0125	19.33	0.065	4.97
3	13.3236	13.4597	3.27	0.029	3.41
4	11.8000	11.9319	3.17	0.031	3.47
5	16.7292	16.7847	1.33	0.027	3.29
6	17.8014	17.8389	0.90	0.024	3.11

Table 3
Table of identified events, having wind speeds above 3.0 m/s at the small meteo buoy. Start time and end time are days of March 1996. Event 1 and 2 are classified as major wind events, the others (3-6) are minor wind events.

Event	Height H_S	Peak frequency	Wavenumber	Stokes drift	Energy
-	[m]	[Hz]	$[m^{-1}]$	[m s^{-1}]	[J m^{-2}]
1	0.43	0.42	0.72	0.070	111.7
2	0.40	0.35	0.50	0.039	95.7
3	0.22	0.45	0.80	0.024	30.2
4	0.022	0.44	0.79	0.000	0.3
5	0.01	0.45	0.83	0.000	0.1

Table 4
Table of wave parameters for the previously identified wind events, having wind speeds above 3.0 m/s. Height H_S is used for significant wave heigth. There are no wave measurements for wind event 6 available. Only the first 3 wind events have significant waveheights above 20 cm.

Run	a0	a1	r	σ	χ^2
r2	-2.02	0.84	0.85	0.016	277.8
r3	-0.97	0.94	0.87	0.016	297.8
r4	-0.65	0.98	0.87	0.017	336.3

Table 5
Results of the linear regression analysis between logarithms of measured and simulated dissipation rates of the uppermost meter (runs r2, r3 and r4). Here a0 denotes the constant, a1 the slope, r the correlation coefficient, σ the standard error of the fit and χ^2 is the value for χ-square-goodness-of-fit test.

event	run r2	run r3	run r4	data
1	-0.97	-1.69	-1.94	-1.85
2	-0.99	-1.71	-1.96	-1.83
3	-0.97	-1.69	-1.83	-2.07
4	-0.96	-1.68	-1.85	-1.81
5	-0.97	-1.69	-1.79	-1.76
6	-1.06	-1.79	-1.87	-1.97

Table 6
Table of mean slope of dissipation rate logarithm versus depth in the uppermost meter for the 6 identified wind events. The slopes for the unmodified $k - \varepsilon$ model are found under run r2, the results from the run r3 are with wave breaking parameterization, results from run r4 are with wave breaking parameterization using an increased surface roughness length and the measurements are under 'data'.

event	ε r2	ε r3	P_S r3	P_B r3	ε r4	P_S r4	ε data
1	1.4	3.5	2.8	2.7e-3	6.4	1.3	11.4
2	3.0	7.6	6.1	7.3e-3	18.1	1.9	19.7
3	0.9	2.4	1.9	5.1e-3	3.0	1.3	5.9
4	0.6	1.6	1.2	1.2e-3	2.0	0.8	1.1
5	0.9	2.2	1.8	-7.0e-3	2.8	1.2	3.5
6	0.7	1.6	1.3	-2.2e-3	1.9	1.0	1.2

Table 7
Table of depth integrated dissipation rate, shear production P_S and buoyancy production P_B of the uppermost meter for the 6 identified wind events. Results are shown from run r2 without wave breaking, run r3 with wave breaking parameterization and from run r4 with increased roughness length z_0. The masured ε is found under 'data'. The units for all quantities is mW/m^2.

event	$\varepsilon - P_S$ r4	P_{wave}	$P_{breaking}$	P_{Stokes}
1	5.1	4.7	14	2.9
2	16.3	2.4	29	2.5
3	1.7	1.6	10	0.7
4	1.2	0.02	11	0.01
5	1.6	0.003	9	0.001

Table 8
Estimated TKE production due to wave breaking from the linear model and according to equation 10 are found under P_{wave} and $P_{breaking}$ respectively. Production because of interaction between Stokes drift and Langmuir circulation is under P_{Stokes}. The units for all quantities is mW/m^2.

9 Figures

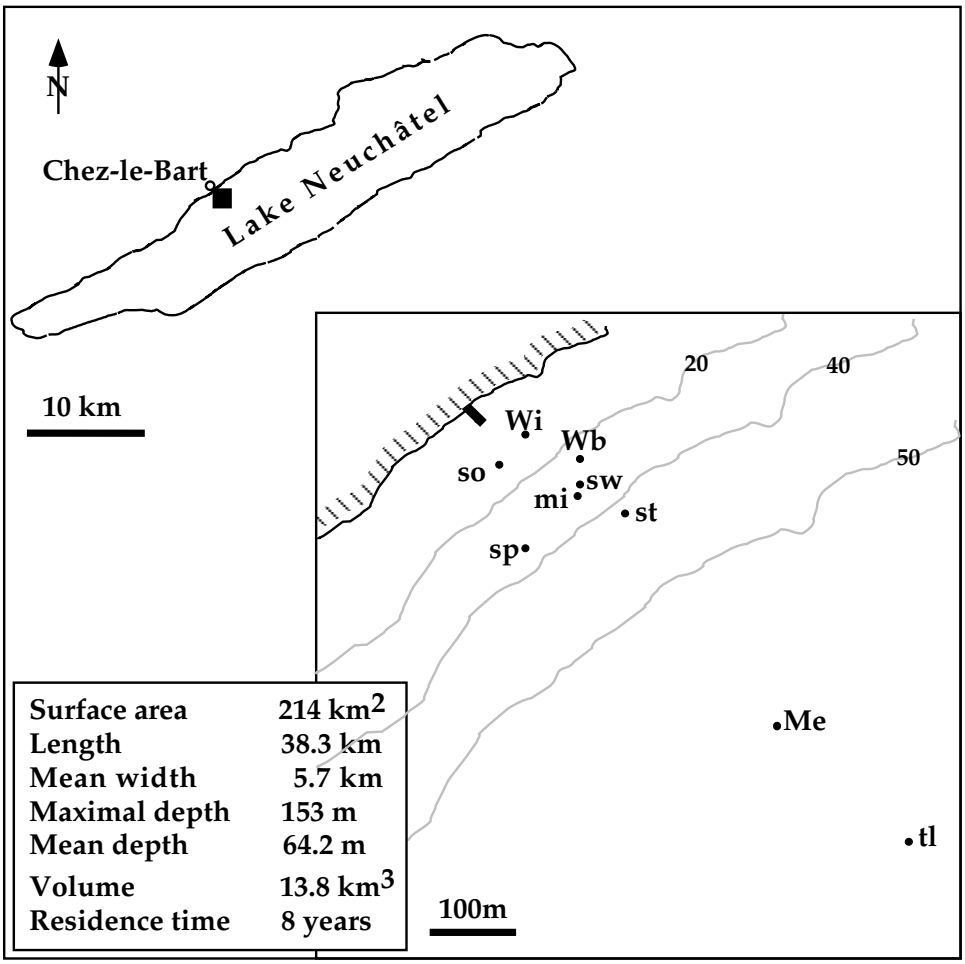

Fig. 1. Lake Neuchâtel, Switzerland. The measurement location is at the shore of Chez le Bart. The meaning of the abbreviations for the different used instruments is given in table 2.

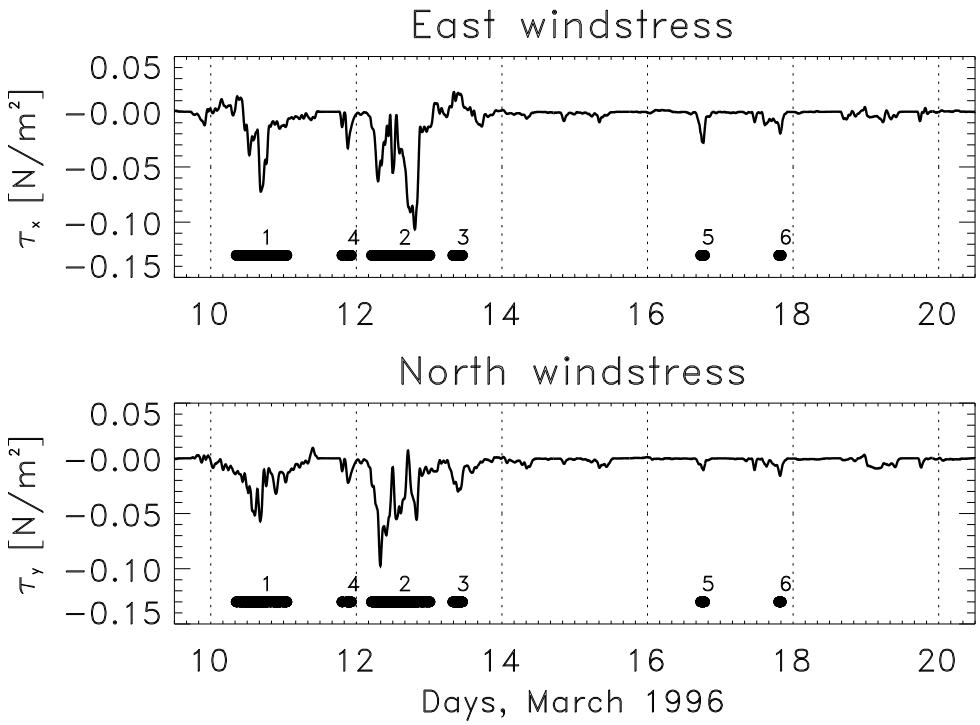

Fig. 2. East wind stress (upper panel) and North wind stress (lower panel) as measured at Lake Neuchâtel. The 6 classified wind events are marked by bold lines and the corresponding number. The two major events (1,2) at 10 and 12 of March can be clearly identified. The long tick marks correspond to the beginning (midnight) of the indicated day.

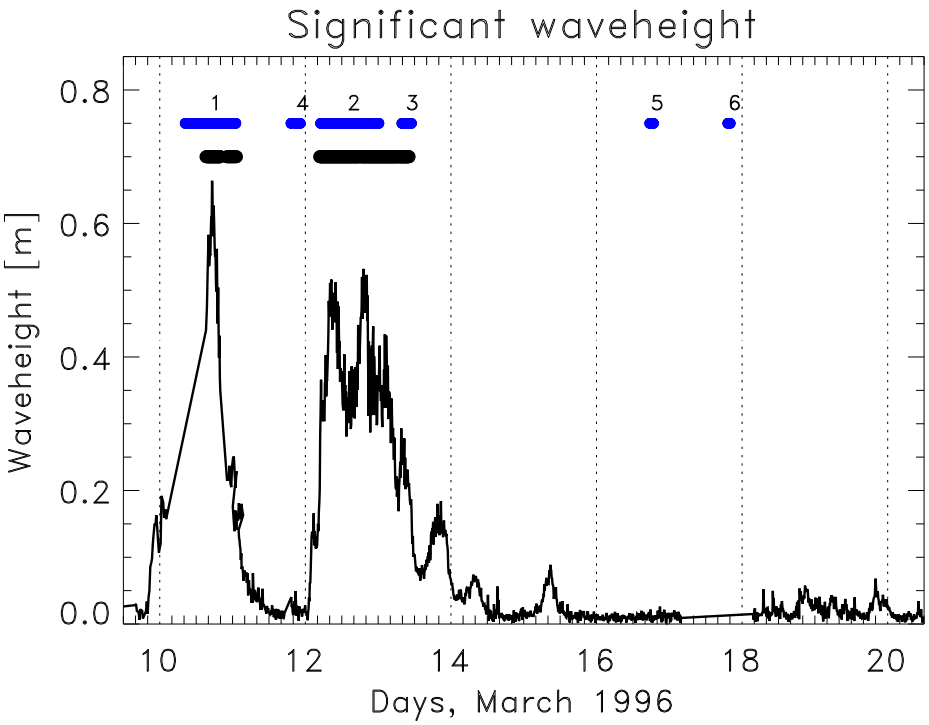

Fig. 3. Significant waveheight H_S measured at about 50 m distance from the turbulence profiling equipment during the Lake Neuchâtel experiment. The 6 classified wind events are marked by the upper bold lines. Two time periods having a significant waveheight H_S of greater than 20 cm are marked by the lower bold lines.

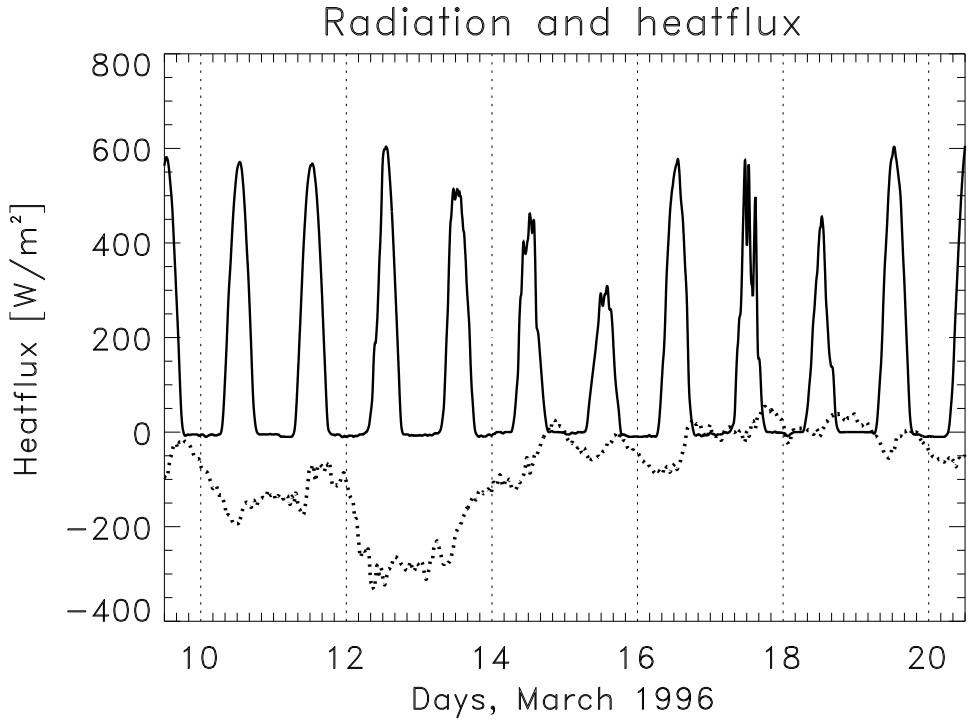

Fig. 4. Short wave radiation (upper solid curve) and surface heat flux (lower dotted curve) as respectively measured and calculated during the Lake Neuchâtel field experiment.

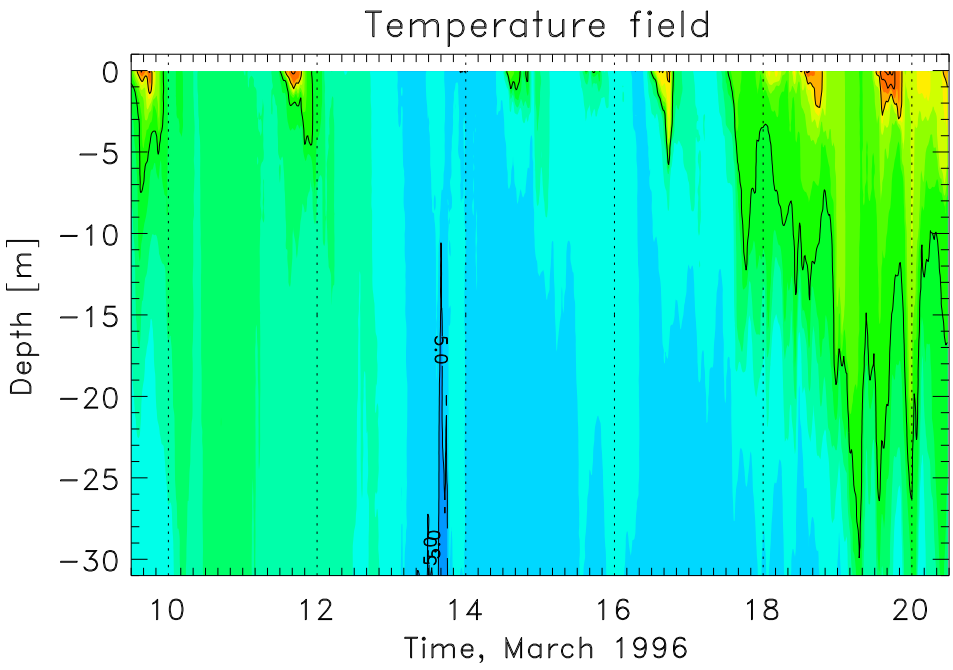

Fig. 5. Contour plot of measured temperature field during the Lake Neuchâtel field experiment. Contours span the range from 5.0 ^oC (blue) to 6.2 ^oC (red).

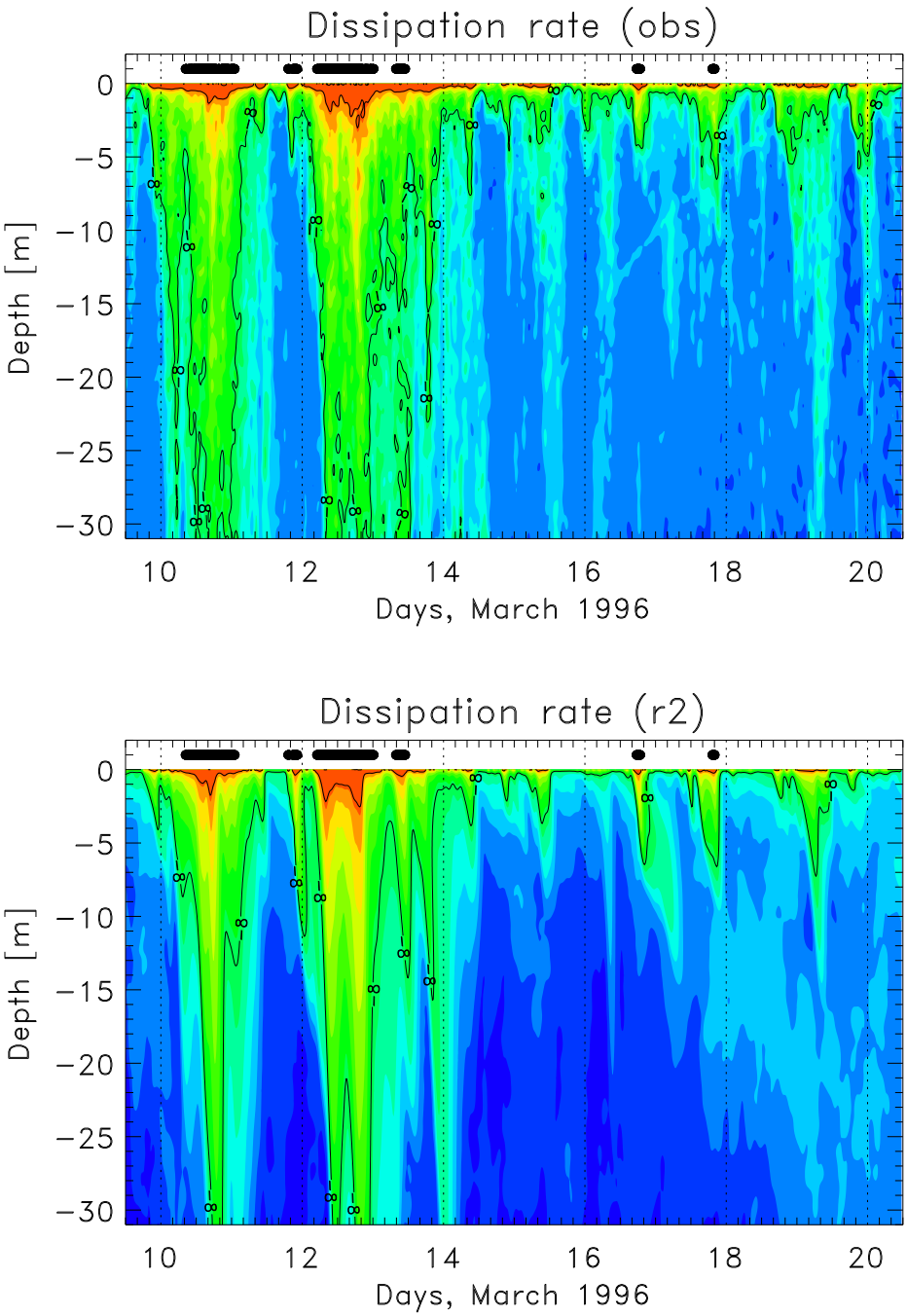

Fig. 6. Contour plots of decadal logarithm of dissipation rate fields, measured (upper panel) and simulated with relaxation run r2 (lower panel). The range is from $log(\varepsilon) = -6$ (red) to $log(\varepsilon) = -10.6$ (dark blue) and the wind events are indicated by the bold lines.

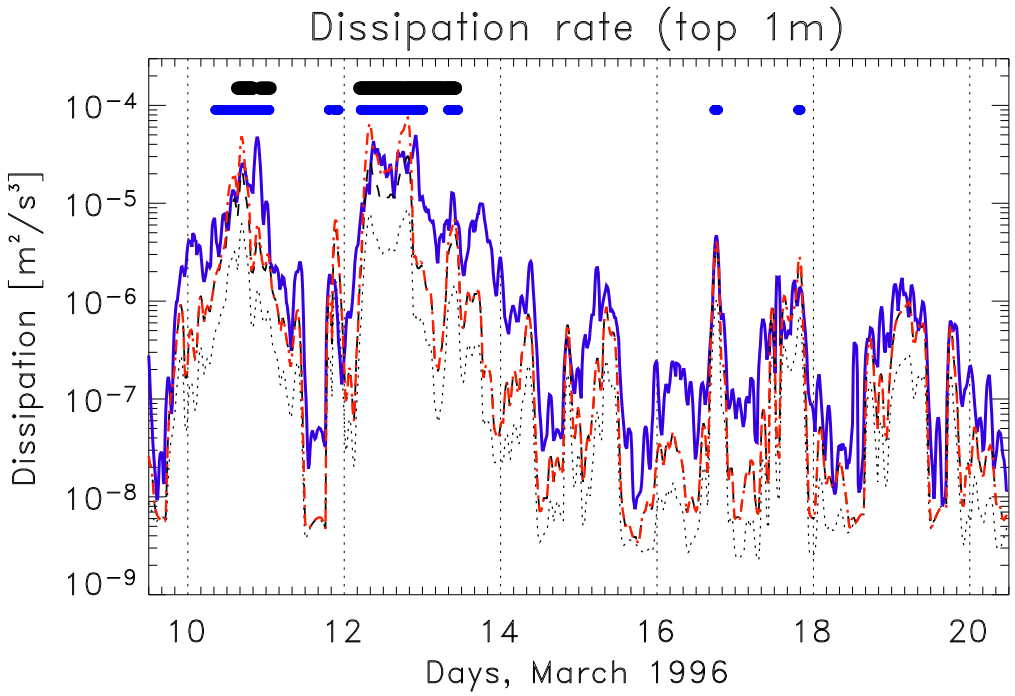

Fig. 7. Mean dissipation rate in the uppermost 1 m, measured (blue solid line), run r2 (dotted line), run r3 (dashed line) and run r4 (red dash-dot line). Except during the strongest winds of event 1 and 2, the results from run r3 and r4 cannot be distinguished. The two major wave events with wave height greater than 20 *cm* are marked bold black. The respective wind events are marked by the smaller bold blue lines.

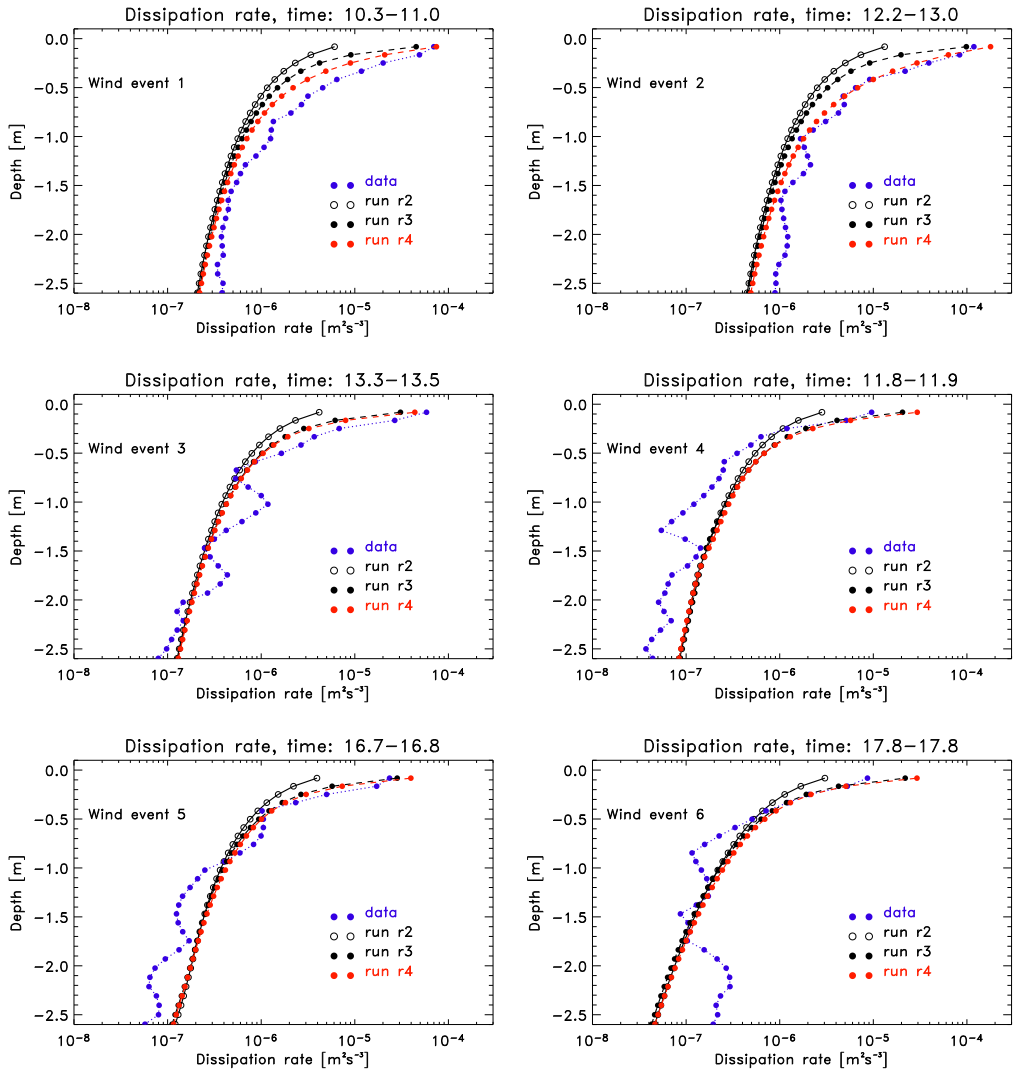

Fig. 8. Near surface profiles of dissipation rate for the selected 6 different wind events. Shown are the results from the simulation without wave breaking (run r2 - black circles), simulation with wave breaking (run r3 - black dots), simulation with increased z_0 (run r4 - red dots) and the observed data (blue dots).

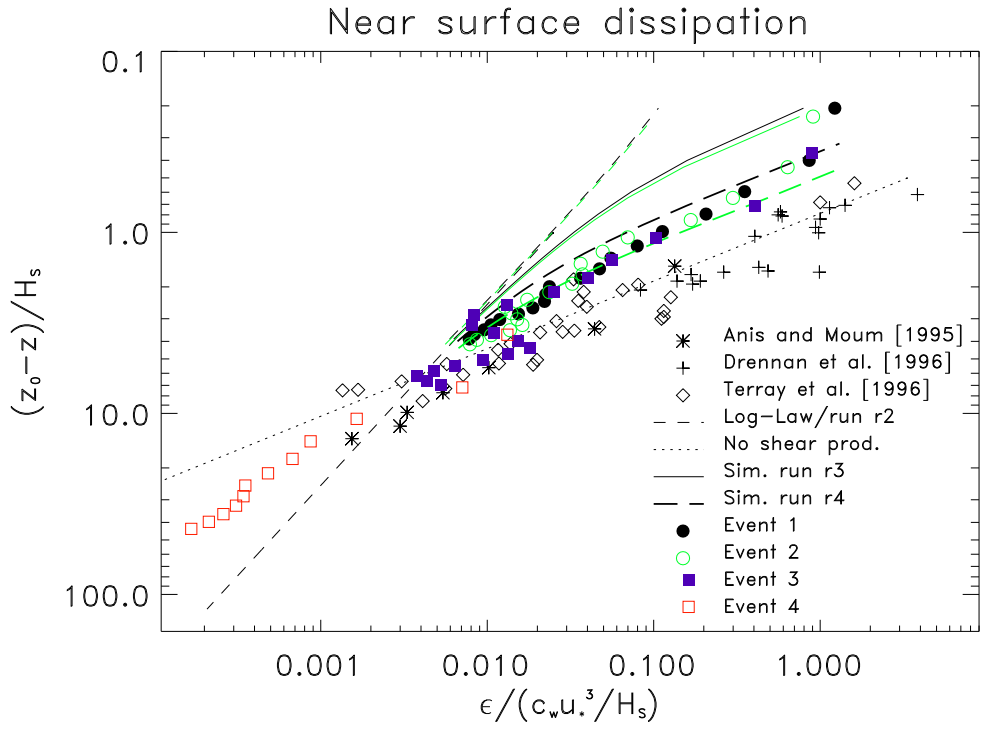

Fig. 9. Nondimensional plot of observations and simulations of dissipation rate in the WASL. All observations are normalized by the surface TKE flux ($C_w u_*^3/H_S$) and the significant wave height H_S. The simulations of run r2 (short dashed lines) coincide with the classical LOW. The pure wave breaking case (no shear production) is shown by the dotted line. Simulations with wave breaking (run r3) are represented by the full lines, whereas the simulation with increased surface roughness length (run r4) is displayed by the longer dashed line. Experimental data are represented by the different symbols and colors. Black lines represent event 1 and green lines event 2.